This is the peer-reviewed, final accepted version for American Mineralogist, published by the Mineralogical Society of America.
The published version is subject to change. Cite as Authors (Year) Title. American Mineralogist, in press.
DOI: https://doi.org/10.2138/am-2020-7500. http://www.minsocam.org/

REVISION 2

Crystal structure of Ag-exchanged levyne intergrown with erionite: single crystal X-ray diffraction and molecular dynamics simulations

Georgia Cametti[1*], Sergey V. Churakov[1,2]

[1]Institute of Geological Sciences, Mineralogical Crystallography, Baltzerstrasse 1+3, 3012 Bern, Switzerland

[2]Paul Scherrer Institut, Forschungstrasse 111, 5232 Villingen PSI, Switzerland

*Corresponding author: georgia.cametti@krist.unibe.ch

ABSTRACT

The modification of natural zeolites *via* ion exchange is an efficient technique used to improve their performances and tune their properties for specific applications. In this study, a natural levyne-Ca intergrown with erionite was fully exchanged by Ag^+ and its structure (with idealized chemical composition $Ag_6(Si,Al)_{18}O_{36}\cdot 18H_2O$) was investigated by combining a theoretical and experimental approach. Single crystal X-ray diffraction data demonstrated that Ag-levyne maintained the *R*-3*m* space group, characteristic of the natural levyne. Ag ions distribute over partially occupied sites along the three-fold axis and, differently from the pristine material, at the wall of the 8-membered ring window of the *lev* cavity. The lack of approximately 30% of Ag ions that could not be located by the structural refinement is ascribed to the strong disorder of the extraframework occupants. The structural results obtained by molecular dynamics simulations are in overall agreement with the experimental data and showed that, on average, Ag^+ is surrounded by approximately 2 H_2O and 1 framework oxygen at distances between 2.43 and 2.6 Å. Molecular dynamics trajectories indicate that the occurrence of silver inside the D6R cage

depends on the water content: silver occupancy of D6R cages is estimated to be 83%, 30%, and 0% when the structure contains 3, 2.5, and 2 H_2O per Ag ion, respectively.

The cation-exchange process, as demonstrated by SEM-EDS analyses affects the intergrown erionite as well. A structural characterization of the Ag-erionite phase (with dimension less than 100 μm) was possible by means of a CuKα micro-focus source: structure solution pointed to $P6_3/mmc$ space group, indicating no change with respect to natural erionite. In agreement with previous studies, K ions in the cancrinite cage could not be exchanged, whereas Ag^+ is found in the *eri* cavity.

Keywords: Zeolites, Ag-levyne, LEV, Ag-erionite, X-ray Diffraction, Molecular dynamics

INTRODUCTION

The mineral series levyne, comprising levyne-Ca and levyne-Na, belongs to the zeolites group. The crystal structure of these minerals is described by a three-dimensional aluminosilicate tetrahedral framework in which charge compensating alkali and/or alkaline earth cations and H_2O occupy the structural voids. Due to their microporous structure, zeolite minerals show interesting properties such as cation exchange, adsorption, reversible hydration/dehydration and the capacity of acting as molecular sieves (Bish and Ming 2001). For this reason, they are successfully applied for a broad range of applications, and in particular in environmental remediation processes (treatment of radioactive wastewater and remediation of contaminated sites (Colella 1999; Babel et al. 2003; Borai et al. 2009; Misaelides 2011; Wang et al. 2010). Compared to their synthetic counterpart, natural zeolites typically show greater thermal stability and better resistance to acid environments (Ackley et al. 2003). Rich opportunities for technological applications, abundance in nature and low mining costs, motivate research on structural and chemical properties of natural zeolites in various scientific disciplines.

LEV-type zeolites are of interest because, despite their small pore openings, they show large micropore volume (0.3 cm^3/g) (Yamamoto et al. 2010). Thus, several phases with **LEV** topology have also been synthesized (Flanigen et al. 1986; Lock et al. 1984; Zhu et al. 1997) and Ca-LEV was suggested as potential hydrogen-storage medium (Liang et al. 2012).

The natural occurring levyne belongs to the so-called ABC-6 family of natural zeolites (Gottardi and Galli, 1985). The **LEV** framework type of levyne is characterized by a sequence of single six-membered rings (6mR) and double six-membered rings (D6R) of tetrahedra stacked along the c axis following the AABCCABBCAA sequence. This sequence originates columns along [001] of cavities [$4^9 6^5 8^3$] (*lev* cavity), which alternates with double six-ring [$4^6 6^2$] polyhedra. Two dimensionally interconnected channels confined by eight-membered rings run perpendicular to [001]. The crystal structure at room temperature is described in *R*-3*m* space group (Merlino et al. 1975; Sacerdoti 1996). Natural crystals of levyne are often twinned by 180° rotation along the c axis simulating *P*6/*mmm* symmetry (Sacerdoti, 1996). Moreover, intergrowths with erionite/offretite, two other zeolites pertaining to the ABC-6 family, have been frequently reported in natural occurring levyne (Shimazu and Mizota 1972; Bennett and Grose 1978; Wise and Tschernich 1976; Passaglia et al. 1974).

The microporous properties of natural zeolites are controlled by the extraframework (EF) cations content. The modification of their crystal-structure *via* cation exchange has been proven to improve their performances over a wide range of applications (Kasture et al. 1998; Ackley et al. 2003; Kanazawa, 2004; Zukal et al. 2010; Amooghin et al. 2016; Ma et al. 2018; Abreu et al. 2019). In particular, Ag-exchanged zeolites show increased sorption and photocatalytic capacity (Hutson et al. 2000; Coutino-Gonzales et al. 2015) and antibacterial efficacy (Milenkovic et al. 2017; Ferreira et al. 2012). To predict the zeolites behavior in terms of stability and microporous

properties two factors are particularly important: i) the position of the EF cations in relation to the aluminosilicate framework, and ii) the modification of the framework itself as a consequence of the EF cations substitution.

In this study, we investigate the crystal structure of Ag-levyne produced by cation exchange of a natural levyne-Ca. In order to determine the EF cation arrangement in the zeolitic channels and to have a better insight into the local environment of silver atoms and global structural disorder, we combined an experimental and theoretical approach. The average structural parameters were determined by means of single crystal X-ray diffraction and compared with that obtained by molecular dynamics simulations. Moreover, a detailed structural characterization of the erionite intergrowths was also undertaken.

MATERIALS AND METHODS

The sample used as starting material was a natural levyne with chemical composition $Ca_{2.53}Na_{0.72}K_{0.23}(Al_{6.26}Si_{11.8}O_{36})\cdot 17.58H_2O$ from Beech Creek, Oregon, USA. The crystals were selected from the same specimen (sample number A7827 of Natural History Museum of Bern) used by Cametti (2018).

The exchange experiments were performed following two steps: at first, levyne crystals with dimensions ranging from 0.08 and 0.3 mm were treated for four weeks with 1M NaCl solution at 100(2)°C in a Teflon autoclave. The solution was renewed every three days. Afterwards, the Na-exchanged crystals were equilibrated with a 2M $AgNO_3$ solution (pH = 5-6) at 100(2)°C for 5 weeks. For this second exchange-step, the crystals were also located in a Teflon autoclave and darkness conditions were maintained during the whole experiment. The $AgNO_3$ solution was periodically renewed every 3 days. The crystals were subsequently removed from the autoclave, washed with deionized water and analyzed by energy-dispersive spectrometry (EDS) using a

ZEISS EVO50 scanning electron microscope (SEM) to ensure the completeness of the exchange process. Operating conditions were 20kV accelerating voltage, 10 mm working distance, 30 s acquisition time. An attempt to analyze the same samples with electron microprobe was not successful due to the small crystal size. Final chemical composition was calculated on the basis of 36 O after renormalization of the chemical analyses hypothesizing a water content of 18% wt.

Single crystal X-ray diffraction (SCXRD)

Diffraction data were collected on a Bruker APEX II diffractometer equipped with a MoKα source (λ = 0.71073) and a CCD detector. A single crystal of Ag-levyne with dimension 0.180 x 0.150 x 0.100 mm was glued on the tip of a glass fiber and mounted on a goniometer head.

The unit cell determination indicated a rhombohedral Bravais-lattice. An inspection of the reciprocal lattice pointed out the presence of an additional set of reflections (approximately 6-7% of the total ones) that could be indexed with the same rhombohedral unit-cell rotated by 180° with respect to the *c*-axis. The data were integrated and corrected for absorption by using the Apex 3v.2018.7-2 software package (Bruker AXS 2017).

The structure was solved in space group *R*-3*m* by direct methods using Shelxtl-2008 (Sheldrick 2008). Structural refinement was carried out by SHELXL-2014 (Sheldrick 2015) by using neutral atomic scattering factors. Starting coordinates and atomic labels of framework atoms were those reported in Sacerdoti (1996) whereas the EF cations and H_2O molecules were located by difference Fourier maps. The obverse-reverse twinning [-100 0-10 001] was refined with fractional volume contribution of 0.058(4).

Erionite and offretite intergrowths have been frequently reported for levyne specimen from the same locality (Bennett and Grose, 1978; Passaglia et al. 1998; Cametti 2018). SEM-BSD pictures of our sample showed the occurrence of another fibrous-mineral phase intergrown between levyne crystals (Fig. 1). To find out whether the intergrown mineral was erionite or offretite and

This is the peer-reviewed, final accepted version for American Mineralogist, published by the Mineralogical Society of America.
The published version is subject to change. Cite as Authors (Year) Title. American Mineralogist, in press.
DOI: https://doi.org/10.2138/am-2020-7500. http://www.minsocam.org/

to determine how this phase was affected by the exchange experiments, single fragments of secondary phase were extracted to perform subsequent structural analyses. Fragments of Ag-exchange levyne were at first carefully inspected under a binocular microscope and disintegrated into smaller pieces with dimensions less than 100 μm. To find the erionite/offretite crystals, several fragments were preliminary checked by single-crystal X-ray diffraction, in order to extrapolate the unit-cell parameters. Finally, a crystal with dimension of approximately 0.05 × 0.03 × 0.015 mm was identified as erionite.

A single crystal of erionite-Ag was glued on the tip of a glass fiber and mounted on a goniometer head. Diffraction data were collected on a Synergy-S Rigaku dual micro-focused source diffractometer equipped with a Hypix detector. The CuKα (λ = 1.54184) radiation was chosen for data collection due to the small dimensions of the crystal under investigation. An attempt to measure the same sample with AgKα, available on the same machine, or with MoKα used for the Ag-levyne X-ray data collection, was not successful because of the low diffracting power of such a small crystal fragment. Diffraction data were integrated and corrected for absorption by using CrysAlisPro 171.40.29a (Rigaku Oxfrod Diffraction, 2018). Erionite crystal structure was solved by direct methods in space group $P6_3/mmc$.

Crystal data, collection and refined parameters are reported in Table S1. Crystallographic information file (Cif) of the refined structures has been deposited as supplementary material. The drawings of the crystal structures were produced by VESTA (Momma and Izumi, 2011).

Molecular dynamics (MD) simulations

Molecular dynamics simulations were performed using the CP2K simulation package (www.cp2k.org). The equations of motion were integrated using a 0.5 fs time step. The interatomic forces were calculated based on Density Functional Theory (DFT) using the Gaussian

and plane waves methods (VandeVondele et al. 2005a). The electron exchange and correlations were described by Perdew-Burke-Ernzerhof functional (PBE) (Perdew et al. 1996). Dispersion interaction was taken into account using the DFT+D2 method (Grimme et al. 2006). The calculations were carried out in NPT ensemble (constant pressure and temperature using a fully flexible cell). Indeed, although atomistic simulations with fixed cell parameters can provide a satisfactory atomistic description of the extraframework content (Gatta et al. 2018), NPT ensemble was chosen in this study to take into account the strong disorder of the EF content and improve the convergence toward the stable configuration.

The simulations temperature of MD was set to 77°C to prevent the glassy behavior of PBE-H_2O (VandeVondele et al. 2005b). The use of slightly elevated temperature makes sure ergodic dynamic of ions and water in the channels. The experimental measurements suggest that the space group symmetry does not change with in the given temperature range. The Kohn-Sham orbitals were expanded using a linear combination of atom centered Gaussian-type orbital functions. A "short-range" double- valence polarized basis set MOLOPT was used for each atomic kind (VandeVondele and Hutter, 2007). Similar setup was successfully used in our previous simulations of zeolites (Cametti et al. 2019a; Cametti et al. 2019b).

The simulation supercell (2 × 1 × 1) contained 684 atoms (36 Ag, 36 Al, 72 O, 216 O, 108 H_2O). The starting coordinates of the framework atoms were those of levyne-Ca (Cametti 2018). Silicon was randomly substituted by aluminum according to the bulk chemical composition following the Loewenstein's rule (Loewenstein, 1954). The Ag atoms were initially placed along the three-fold axis parallel to [001] in the middle of each [$4^9 6^5 8^3$] cavity. The number of H_2O was set according to the idealized chemical composition of levyne that is 3.0 H_2O per EF cation (Passaglia and Sheppard, 2001). The structural data were collected from a 25 ps-long MD trajectory followed by

at least 6 ps pre-equilibration. Moreover, two additional structural models with 2.5 and 2 H_2O per Ag atom, respectively, were tested.

RESULTS

The EDS-SEM analyses of the Ag-exchanged levyne showed that Na^+ was completely replaced by Ag^+. The detected amount of potassium was related to the occurrence of erionite intergrowths as confirmed by SEM pictures (Fig. 1). Within the same single crystal, two main domains can be recognized: one with a fibrous-like morphology, which mainly contains K and Ag as EF cations and, the other that is K-free. This kind of intergrowths, i.e. erionite on the {0001} faces of levyne lamellae is frequent and was observed in samples from different localities (Passaglia et al. 1974; Bennet and Grose, 1978; Wise and Tschernich, 1976; Gottardi and Galli, 1985). Final chemical composition for Ag-levyne and -erionite are $Ag_{6.1}Al_{6.3}Si_{11.8}O_{36}\cdot 18.0H_2O$ and $Ag_{8.9}K_{1.7}Al_{10.1}Si_{22.5}O_{72}\cdot 30H_2O$, respectively.

Crystal structure of Ag-levyne

The Ag-levyne structure at RT preserves the space group *R*-3*m* characteristic of the natural levyne-Ca. The aluminosilicate framework did not show significant changes because of Ag^+ uptake. The unit cell parameters were comparable with those of the pristine material (Cametti, 2018). The dimension (6.48 × 7.39 Å) of the apertures of the 8-membered ring channels along [100] was similar to that of levyne-Ca (6.44 × 7.42 Å).

The structural refinement of the XRD data indicated that Ag ions are strongly disordered within the zeolitic pores. Four main EF Ag sites (Ag1, Ag2, Ag3, and Ag4) were located plus additional low-occupied sites (Ag1A, Ag2A, Ag2B, Ag4A,…Ag4E) (occupancy less than 0.15) close to the main ones (Fig. 2, Table S2). The Ag1 site is the most populated, with occ. = 0.429(19). In Ag-

186 levyne, the Ag sites (Ag1, Ag2, and Ag3) are distributed along the 3- fold axis and, different to
187 the EF cations in natural levyne-Ca, at the wall of the eight-membered ring window of the *lev*
188 cage (Ag4) (Fig. 2). Ag ions at this position are extremely disordered and a simultaneous
189 presence of Ag and H_2O cannot be excluded.
190 In natural levyne-Ca (Cametti, 2018), EF cations and H_2O are found at five sites: (C1, C2, C3,
191 C4, C5) and (W1, W2, W3, W4, and W5), respectively. In Ag-levyne:

192 • Ag1 site corresponds to C1 that in levyne-Ca is almost fully occupied by Ca;
193 • Ag3 site corresponds to C2, which in levyne-Ca is 13% occupied by Ca;
194 • Ag2, Ag2A, and Ag2B correspond to C3, C4, and C5 respectively; these positions in
195 natural levyne-Ca, are partially occupied by Na, K, and Ca respectively (Cametti, 2018).
196 • The positions of Ag4 sites (Ag4A, Ag4B, Ag4C, Ag4D, and Ag4E) are comparable to
197 those of H_2O at W2, W4, and W5 in levyne-Ca;
198 • W1 and W3 positions are identical in levyne-Ca and Ag-levyne.

199 Relevant bond distances of Ag-levyne structure are reported in Table 1. Ag1 site is coordinated
200 by three H_2O at W1 (2.372(8) Å) and three framework-oxygen atoms at O2 (2.470(5) Å),
201 forming a fairly regular octahedron. Ag2 site bonds to six framework-oxygen atoms at O5
202 (2.591(5) Å), which constitute the aperture of the six-membered ring window of the *lev* cavity.
203 Bond distances between 2.24 and 2.6 Å are found for Ag4A, Ag4B, Ag4C, Ag4D, and Ag4E. On
204 average, the sites at these positions bond to three oxygen atoms of the 8-membered ring aperture
205 (two at O1 and one at O3) and two H_2O at W3.

206 The total number of Ag ions per formula unit obtained by the structural refinement was lower
207 compared to that estimated by the chemical analyses. On the basis of 36 oxygen, the total
208 number of positive charges required to balance the negative charge of the aluminosilicate

This is the peer-reviewed, final accepted version for American Mineralogist, published by the Mineralogical Society of America.
The published version is subject to change. Cite as Authors (Year) Title. American Mineralogist, in press.
DOI: https://doi.org/10.2138/am-2020-7500. http://www.minsocam.org/

framework is 6. However, if all the EF sites are refined with Ag scattering factor, the refined Ag^{+} apfu is only 4, pointing out that approximately 30% of the EF silver could not be located by XRD.

Molecular dynamics

The unit lattice constants obtained by MD simulations are close to those obtained by XRD, with a deviation of less than 1% for all parameters and 1.75% for the length of the c-axis (Table 2).

Fig. 3 reports a snapshot of the structure obtained after 20 ps calculation. Ag atoms are found mainly along the three-fold axis and part of them are displaced toward the 8-membered ring window of the *lev* cavity. The radial distribution function (RDF) and running coordination number (CN) of the Ag-O (O oxygen of the framework) and Ag-Ow (Ow oxygen of the H_2O) are reported in Fig. 4. The RDF of the Ag-Ow distances show a clear peak at 2.43 Å, whereas the curve corresponding to Ag-O indicates a broadened distribution of distances with a maximum at ca. 2.5 Å. On average, each Ag is surrounded by approximately 2 H_2O and 1 framework oxygen at distances between 2.43 and 2.60 Å.

The Ag ions in the *lev* cavity are found at the top and bottom of the cavity, close to the aperture of the six-membered rings (Fig. 5a). These atoms are coordinated by three-framework oxygens and by three H_2O, which occupy the central part of the cage. Additional Ag ions, located at the 8-memebred ring windows, bond to two framework oxygen atoms and to two or three H_2O (Fig. 5a). Such Ag distribution in the *lev* cavity agrees with that observed by the structural refinement (Fig. 5b) where Ag ions disordered at Ag4 sites are located on the wall of the aperture of the 8-membered ring. Additional disordered Ag atoms at Ag2 sites are distributed at the bottom of the cage.

This is the peer-reviewed, final accepted version for American Mineralogist, published by the Mineralogical Society of America.
The published version is subject to change. Cite as Authors (Year) Title. American Mineralogist, in press.
DOI: https://doi.org/10.2138/am-2020-7500. http://www.minsocam.org/

In the simulations setup with 3 H_2O per Ag atom, an additional Ag ion is found at (0,0,0), in the middle of approximately 83% of the double six-membered rings (D6R) cage (Fig. 3). In contrast, in the structural refinement, no residual electron density was found at this position and an attempt to insert an additional site at (0,0,0) was not successful.

The hydrogen bond-net of the structure with 3 H_2O mainly involves oxygen of the water molecules whereas no significant interactions between H and framework oxygens was observed (each O has approximately only 0.2 H atoms within 2.0 Å Fig. S1). The RDF and CN of Ow···H contacts shows that, on average, 0.5 H are found at distance of 1.70 Å from Ow, indicating a medium-strong character of such interactions (Fig. S1). As expected, the number of the Ow···H contacts decreases and becomes less significant if the modelled structures with 2 and 2.5 H_2O per Ag ion are considered (Fig. S2). Detailed analysis of the Ow-H RDF shows that in agreement with expected more acidic properties of the H_2O coordinating the Ag-ion, proton donation events take place between water in Ag-coordination shell and interstitial water (Albuquerque and Calzaferri, 2007; Fois and Tabacchi, 2019).

Crystal structure of intergrown Ag-erionite

The structural parameters of Ag-exchanged erionite and relevant bond distances are reported in Table S3 and Table 3, respectively. The $P6_3/mmc$ characteristic of the natural erionite (Alberti et al. 1997) is preserved after the uptake of Ag ions. The unit-cell (a = 13.29919(19), c = 15.19312(19) Å, V = 2327.17(7) $Å^3$) is slightly smaller compare to that of an erionite sample from the same locality (a = 13.345(1), c = 15.124(3) Å, V = 2332.6(5) $Å^3$) reported by Passaglia et al. (1998). According to the structural refinement, K occupies the middle of the cancrinite cage, where it is slightly displaced along z direction as demonstrated by the occurrence of an additional site K1A (Occ. = 0.030(16)) at 0.8(3) Å from K1 (Occ. =0.98(4)) (Fig. 6). This finding

is in agreement with Sherry (1979) who reported that potassium in the cancrinite cavities cannot be replaced via ion exchange in aqueous solution because of the small opening of the 6-membered ring window, which hampers the passage of the K ions.

Ag ions are distributed in the *eri* cavity, at disordered sites with partial occupancies (Fig. 6). Three main positions can be recognized:

- C1, the most occupied site (Occ. = 0.679(14)) is located in the erionite cavity close to the 6-membered ring aperture of the cancrinite cage; it forms two bonds with framework oxygen at O6 (2.500(6) Å) and two longer connections (2.986(5) Å) with those at O4. A very low occupied site C1A close to C1 indicates, also in this case, a displacement from the mirror plane perpendicular to [001].
- C2, disordered at three different subsites (C2, C2A, C2B, with total Occ. = 0.53) distributes at the bottom and top of the erionite cavity, in the aperture center of the 6-membered rings. Ag ions at this position form bonds with framework oxygen O5 of the six-membered ring and with H_2O at W5 site, which is located along the three-fold axis.
- C3, C3A, and C3B (total Occ. = 0.21) are located in the middle of the *eri* cavity and bond only to H_2O at W5A and W4A.

All water molecules, but those at W5 and W5A, are distributed over five sites at the wall of the *eri* cavity in correspondence of the 8-membered ring window (Table S3, Fig. 6).

The total number of positive charges obtained by the structural refinement (11.3^+) is in reasonable agreement with that estimated by the chemical analysis (12.3^+).

DISCUSSION

The analysis of the erionite intergrowths demonstrated that all EF cations in the *eri* cavity could be exchanged with Ag^+ and, differently from Ag-levyne, all Ag ions in the unit cell could be

located by the structural refinement. The lack of ca. 30% of Ag^+ in Ag-levyne structure can be explained by: (i) migration of part of silver toward the external surface or (ii) strong disorder of the remaining Ag^+ in the structural voids, which prevents its exact location.

Since positional disorder of EF sites was observed also in Ag-erionite, but all Ag could be located, we decided to collect additional XRD data on Ag-levyne by using the more brilliant Cu micro-focused source employed to investigate Ag-erionite. Other two fragments of Ag-levyne were selected and data were collected on the same instrument used for Ag-erionite. As an example, data-collection parameters and results obtained for the first fragment are reported in Table S4 and S5. Structural refinements did not show any significant change in terms of EF cation positions but, in both cases, the refined chemical composition indicated an Ag content higher than 5 apfu. Such a value can be reasonably accepted, if the errors on refined values of both occupancies and thermal parameters are taken into account (Table S5). Thus, the disorder hypothesis (ii) seems the most reasonable. Such hypothesis is also supported by similar findings in hydrated fully-exchange Ag-chabazite and Ag-heulandite (Nevenka et al. 1981; Calligaris et al. 1983). In both cases, the authors could not locate by XRD methods all Ag ions revealed by the chemical analyses. In Ag-exchanged heulandite, only 56 % of exchanged Ag^+ were detected by X-ray (Nevenka et al., 1981). Similarly, in Ag-chabazite only 61% Ag^+ could be placed by the structural refinement (Calligaris et al. 1983). The interpretation given by the authors was that remaining Ag ions "spread out in the channels of the zeolite … giving no detectable contribution to the diffraction pattern" (Nevenka et al. 1981).

According to our findings, the distribution of Ag^+ in the two intergrown phases slightly differs. In erionite, the disorder that affects the Ag ions is less pronounced; with the exceptions of C1A and C3A, and C3B sites, the occupancies of all EF sites is higher than 0.15, and most part of Ag is

found at C1 site (Occ. = 0.679(14)). In Ag-levyne, apart from Ag1 (Occ. = 0.429(19)), ions are distributed at sites with occupancies less than 0.15. In particular, silver ions at the wall of the *lev* cavity are significantly disordered and affected by high displacement parameters that strongly influence the final values of the refined occupancies.

Overall, the exchange of the original EF cations with Ag^+ in the levyne structure does not induce significant structural modifications of the framework. The Ag^+ ions distribute at different crystallographic sites compared to levyne-Ca and to levyne-Na. In particular, the sites at Ag4-Ag4E sites are located at the aperture of the 8-membered rings of the *lev* cavity where in natural levyne H_2O molecules are found. Such distribution was confirmed by the MD simulations, which indicated a displacement of the EF cations away from the 3-fold axis. MD trajectories also pointed out the occurrence of a silver ion located inside the D6R cage. However, according to XRD results, no residual electron density was found at this position.

To explain this mismatch, we have to keep in mind that in real exchange experiments, not only the availability but also the accessibility of the EF sites must be considered; the latter is related to the kinetic behavior of the ion-exchange system and thus to the diffusion coefficients of that specific ion within the pores (Inglezakis et al. 2004). The diffusion and the ability of an ion to access a specific site may depend on its hydration shell. From the structural refinement, we could not unambiguously determine the exact water content, due to the strong disorder of the EF occupants. MD simulations with 3 H_2O per Ag ion, represent an idealized chemical composition of levyne-$(Ca_{0.5},Na)_6$ (Passaglia and Sheppard, 2001). However, in Ag-levyne, the number of EF cations is 1.5 greater than in levyne-Ca (1 Na plus 2.5 Ca apfu). A possible reason of the presence of Ag^+ inside the D6R cage could be the overestimation of the number of structural

This is the peer-reviewed, final accepted version for American Mineralogist, published by the Mineralogical Society of America.
The published version is subject to change. Cite as Authors (Year) Title. American Mineralogist, in press.
DOI: https://doi.org/10.2138/am-2020-7500. http://www.minsocam.org/

H_2O; less room for Ag ions in the *lev* cavity, would force them to enter inside the D6R cage. To test the effect of H_2O amount on the Ag distribution in **LEV** framework type, additional molecular dynamics simulations (12 ps long trajectories) of Ag-levyne structure with different water content were performed. At first, we hypothesized 2.5 H_2O (instead of 3) per Ag ion that is 15 H_2O pfu. With such configuration, only 30% of the D6R cage is occupied by a Ag ion. When removing an additional 0.5 H_2O, i.e. modelling a structure with only 2 H_2O per Ag ion (12 H_2O pfu) no EF cations are found inside the cage at (0,0,0) (Fig. 7). In both cases, displacement of part of Ag ions from the three-fold axis toward the 8-membered ring window was observed.

Based on these results, the structure containing 2 H_2O per Ag ion represents the best agreement between experimental (XRD) and calculated (MD) Ag-levyne. It should be kept in mind that the amount of structural (and absorbed) water in a zeolitic material is strongly influenced by the environmental conditions the sample is exposed to (i.e. relative humidity, temperature). It is worth to mention, that in one of the data set collected as test purpose (by using the Cu micro-focus source) on a fragment of Ag-levyne, a tiny peak at (0,0,0) appeared in the difference Fourier maps. Nevertheless, an attempt to insert it in the structural refinement did not lead to satisfactory results, being the refined value as big as the computed error. Interestingly, the occurrence of a cation at this position, i.e. (0,0,0), was found in the dehydrated form of levyne-Ca (Arletti et al. 2013, Cametti, 2018).

IMPLICATIONS

Currently, natural zeolites are effectively applied for waste-water treatment and removal of contaminants. On the other hand, their use in other important fields such as catalysis or gas separation processes is still limited. In the last decades, much effort has been made to improve

348 the catalytic and separation potential. The functionalization and modification of the natural
349 zeolites by thermal treatment or ion-exchange has been one of the most used and successful
350 technique (Zukal et al. 2010; Ma et al. 2017; Abreu et al. 2019; Velazquez-Pena et al. 2019). The
351 specific case of Ag-modified zeolites is particularly interesting, because silver is known to
352 strongly influence the adsorption characteristics of aluminosilicate zeolites (Hutson 2000). For
353 example, modified Ag-ferrierite and Ag-mordenite are applied in air purification processes
354 (Ar/O_2 enrichment or exhaust gas cleanup) (Knaebel and Kandybin, 1993; Ogawa et al. 2001). In
355 addition, Ag-exchanged zeolites have attracted great attention due their remarkable luminescent
356 and photocatalytic properties (De Cremer et al. 2009; Countino-Gonzales et al. 2015; Aghakhani
357 et al. 2018). In this context, particular attention must be paid not only to the framework topology
358 and to the size of the micro pores but also, and especially, to the cation positions in the structural
359 voids (Seifert et al. 2000; Aghakhani et al. 2018; Fron et al. 2019). Previous researches on
360 transition-metals modified zeolites have shown that even if the structure experiences little
361 modifications of the framework at RT, the new EF cations have a significant influence on the
362 dehydration path (i.e. phase transformations) and thermal stability of the new-produced zeolite.
363 With this respect, a high temperature structural study is in progress to check whether Ag-levyne
364 will undergo, upon heating, different structural changes compare to levyne-Ca.
365

366 **Acknowledgement**

367 We are thankful to Dr. Beda Hoffman of Natural History Museum of Bern who provided the
368 levyne sample, Dr. Mariko Nagashima for her help with EMPA analyses, and to Thomas
369 Armbruster for reading the manuscript. We acknowledge access to the Swiss National
370 Supercomputing Center (CSCS) and UBELIX HPC cluster at the University of Bern. The Swiss
371 National Science Foundation (SNF) is acknowledged for the Ambizione grant n. PZ00P2 173997

awarded to G. C. and for the R'Equip grant n. 206021_177033 awarded to P. Macchi. Gloria Tabacchi and an anonymous reviewer are thanked for their very constructive comments.

REFERENCES

Abreu, N. J., Valdés, H., Zaror, A. C., Azzolina-Jury, F., Meléndrez, M. F. (2019) Ethylene adsorption onto natural and transition metal modified Chilean zeolite: An *operando* DRIFTS approach. Microporous and Mesoporous Materials, 274, 134-148.

Ackley, M. W., Rege, S. U., Saxena, H. (2003) Application of natural zeolites in the purification and separation of gases. Microporous and Mesoporous Materials, 61, 25-42.

Aghakhani, S., Grandjean, D., Baekelant, W., Coutiño-Gonzales, E., Fron, E., Kvashnina K., Roeffaers M. B. J., Hofkens, J., Sels, B. F., Lievens, P. (2018) Atomic scale reversible opto-structural switching of few atom luminescent silver clusters confined in LTA zeolites. Nanoscale, 10, 11467-11476.

Alberti, A., Martucci, A., Galli, E., Vezzalini, G. (1997) A re-examination of the crystal structure of erionite. Zeolites, 19, 349-352.

Albuquerque, R. Q., Calzaferri, G. (2007) Proton activity inside the channels of zeolite L. Chemistry, a European Journal, 13, 8939-8952.

Amooghin, A. B., Omidkhah, M., Sanaeepur, H., Kargari, A. (2016) Preparation and characterization of Ag+ ionexchanged zeolite-Matrimid® 5218 mixed matrix membrane for CO_2/CH_4 separation. Journal of Energy Chemistry, 25, 450-462.

Arletti, R., Vezzalini, G., Quartieri, S., Cámara, F., Alvaro, M. (2013) A new framework topology in the dehydrated form of zeolite levyne. American Mineralogist, 98, 2063-2074.

Babel, S., Kurniawan, T. A. (2003) Low-cost adsorbents for heavy metals uptake from contaminated water: a review. Journal of Hazardous Material, 97, 219-243.

Bennett, J. M., Grose, R. W. (1978) Characterization of the offretite-levynite intergrowth from Beech Creek, Oregon, by adsorption and electron diffraction. In: Sand L. B., Mumpton, F. A., (eds) Natural Zeolites. Pergamon, Oxford, pp 77-84.

Bish, D. L; Ming, D. W. *Natural zeolites: occurrences, properties and applications.* Reviews in Mineralogy and Geochemistry, 45. Mineralogical Society of America and Geochemical Society, Washington DC, 2001.

Borai, E. H., Harjula, R., Malinen, R., Paajanen, A. (2009) Efficient removal of cesium from low-level radioactive liquid waste using natural and impregnated zeolites minerals. Journal of Hazardous Material, 172, 416-422.

Bruker AXS, APEX3 v2019.1-0.

Calligaris, M., Nardin, G., Randaccio, L. (1983) Cation site location in hydrated chabazites. Crystal structure of potassium- and silver-exchanged chabazites. Zeolites, 3, 205-208.

Cametti, G. (2018) New topology of levyne B under quasi-equilibrium conditions: A temperature-dependent in situ single crystal X-ray diffraction study. Microporous and Mesoporous Materials, 265, 162-171.

Cametti, G., Scheinost, A. C., Churakov, S. V. (2019b) Structural modifications and thermal stability of Cd^{2+}-exchanged stellerite, a zeolite with STI framework type. Journal of Physical Chemistry C, 123, 25236-25245.

Cametti, G., Scheinost, A. C., Giordani, M., Churakov, S. V. (2019a) Framework modifications and dehydration path of a Ag^{+}-modified zeolite with STI framework type. Journal of Physical Chemistry C, 123, 13651-13663.

Colella, C. Environmenal applications of natural zeolitic materials based on their ion-exchange properties, in: P. Misaelides, F. Macasek, T. J. Pinnavaia, C. Colella (Eds.), *Application of natural microporous materials in environmental technology, Kluwer, NATO Science Series vol. E362* (Applied Sciences), Dordrecht, 1999.

Coutino-Gonzales, E., Baekelant, W., Grandjean, D., Roeffaers, M. B. J., Fron, E., Aghakhani, M. S., Bovet, N., Van der Auweraer, M., Lievens, P., Vosch, T. et al. (2015) Thermally activated LTA(Li)-Ag zeolites with water-responsive photoluminescence properties. Journal of Material Chemistry C, 3, 11857-11867.

CP2K developers group. http://www.cp2k.org, 2000-2019.

CrysAlisPro, Rigaku Oxford diffraction, 2018, Version 171.40.29a.

De Cremer, G., Coutino-Gonzales, E., Roeffaers, M. B. J., Moens, B., Ollevier, J., Van der Auweraer, M., Schoonheydt, R., Jacobs, P. A., De Schryver, F. C., Hofkens, J., De Vos, D. E., Sels, B. F., Vosch, T. (2009) Characterization of fluorescence in heat-treated silver-exchanged zeolites. Journal of American Chemical Society, 131, 3049-3056.

Ferreira, L., Fonseca, A. M., Botelho, G., Aguiar, C. A., Neces, I. C. (2012) Antimicrobial activity of faujasite zeolites doped with silver. Microporous and Mesoporous Materials, 160, 126-132.

Flanigen, E. M., Lok, B. M., Patton, R. L., Wilson, S. T. (1986) Aluminophosphate molecular sieves and the periodic table. Pure and Applied Chemistry, 58, 1351-1358.

Fois, E., Tabacchi, G. (2019) Water in zeolite L and its MOF mimic. Zeitschrift für Kristallographie - Crystalline Materials, 234, 2018-2153.

Fron, E., Aghakhani, S., Baekelant, W., Grandjean, D., Coutino-Gonzales, E., Van der Auweraer, M., Roeffaers, M. B. J., Lievens, P., Hofkens, J. (2019) Structural and photophysical characterization of Ag clusters in LTA zeolites. Journal of Physical Chemistry C, 123, 10630-10638.

Gatta, G. D., Lotti, P., Tabacchi, G. (2018) The effect of pressure on open-framework silicates: elastic behaviour and crystal-fluid interaction. Physics and Chemistry of Minerals, 45, 115-138.

Gottardi, G.; Galli, E. *Natural zeolites*; Springer-Verlag Berlin Heidelberg, New York Tokyo, 1985.

Grimme, S. (2006) Semiempirical GGA-Type Density Functional Constructed with a Long-Range Dispersion Correction. Journal of Computational Chemistry, 27, 1787-1798.

Hutson, N. D., Reisner, B. A., Yang, R. T., Toby, B. H. (2000) Silver ion-exchanged zeolites Y, X, and low-silica X: Observations of thermally induced cation/cluster migration and the resulting effects on the equilibrium adsorption of Nitrogen. Chemistry of Materials, 12, 3020-3031.

Inglezakis, V. J., Loizidou, M. M., Grigoropoulou, H. P. (2004) Ion exchange studies on natural and modified zeolites and the concept of exchange site accessibility. Journal of Colloid and Interface Science, 275, 570-576.

Kasture, M. W., Joshi, P. N., Sorti, H. S., Joshi, V. V., Choudhari, A. L., Shiralkar, V. P. (1998) Sorption properties of the natural, K and partially deammoniated (H/NH4) forms of clinoptilolite. Adsorption Science and Technology, 16,135-151.

459 Kanazawa, T. (2004) Development of hydrocarbon adsorbents, oxygen storage materials for three-
460 way catalysts and NOx storage-reduction catalyst. Catalysis Today, 96, 171-177.

461 Knaebel, K. S., Kandybin, A. (1993) Pressure swing adsorption system to purify oxygen. US patent
462 5,226,933.

463 Liang, J., Zhang, R., Zhao, Q., Dong, J., Wang, B., Li, J. (2012) Molecular simulation of hydrogen
464 storage in ion-exchanged mazzite and levyne zeolites. Computational and Theoretical
465 Chemistry, 980, 1-6.

466 Loewenstein, W. (1954) The distribution of aluminum in the tetrahedra of silicates and aluminates.
467 American Mineralogist, 39, Nr. 1/2, S. 92.

468 Lock, B. M., Messina, C. A., Patton, R. L., Gjek, R. T., Cannan, T. R., Flanigen, E. M. (1984) U.S.
469 Patent 4,440,871.

470 Ma, Z., Zhang, Q., Weng, X., Mang, C., Si, L., Guan, Z., Cheng, L. (2018) Fluoride ion adsorption
471 from wastewater using magnesium(II), aluminum(III) and titanium(IV) modified natural
472 zeolite: kinetics, thermodynamics, and mechanistic aspects of adsorption. Journal Water
473 Reuse and Desalination, 8, 479-489.

474 Merlino, S., Galli, E., Alberti, A. (1975) The crystal structure of levyne. Tschermaks
475 Mineralogische und Petrographische Mitteilungen, 22, 117-129.

476 Milenkovic, J., Hrenovic, J., Matijasevic, D., Niksic, M., Rajic, N. (2017) Bactericidal activity of
477 Cu-, Zn-, Ag-containing zeolites toward Escherichia coli isoltates. Environmental Science
478 and Pollution Research, 24, 20273-20281.

479 Misaelides, P. (2011) Application of natural zeolites in environmental remediation: A short review.
480 Microporous and Mesoporous Material, 144, 15-18.

Momma, K., Izumi, F. (2011) VESTA 3 for three-dimensional visualization of crystal, volumetric and morphology data. Journal of Applied Crystallography, 44, 1272-1276.

Nevenka, B. P., Calligaris, M., Nardin, G., Randaccio, L. (1981) Location of cations in metal ion-exchanged Zeolites. Part 2. Crystal structures of a fully silver-exchanged heulandite. Journal of the Chemical Society, Dalton Transactions, 12, 2288-2291.

Ogawa, H., Ito, Y., Nakano, M., Itabashi, K. (2001) Method for adsorbing and removing ethylene and method for purifying an exhaust gas. US patent 6,309,616.

Passaglia, E., Artioli, G., Gualtieri, A. (1998) Crystal chemistry of the zeolites erionite and offretite. American Mineralogist, 83, 577-589.

Passaglia, E., Galli, E., Rinaldi, R. (1974) Levynes and erionites from Sardinia. Contributions to Mineralogy and Petrology, 43, 253-259.

Passaglia, E., Sheppard, R. A. (2001) The crystal chemistry of zeolites. In: D. L. Bish and D. W. Ming, Eds., Natural Zeolites: Occurrence, Properties, Applications, vol. 45, p. 70-116. Reviews in Mineralogy and Geochemistry, Mineralogical Society of America, Chantilly, Virginia.

Perdew, J. P., Burke, K., Ernzerhof, M. (1996) Generalized gradient approximation made simple. Physical Reviews Letters, 77, 3865-3868.

Sacerdoti, M. (1996) New refinements of the crystal structure of levyne using twinned crystals. Neues Jahrbuch für Mineraolige Monatshefte, 3, 114-124.

Seifert, R., Rytz, R., Calzaferri, G. (2000) Colors of Ag^{+}-Exchanged Zeolite A. Journal of Physical Chemistry A, 104,7473-7483.

Sheldrick, G. M. (2008) A short history of SHELX. Acta Crystallographica A, 64, 112-122.

503 Sheldrick, G. M., Crystal structure refinement with SHELXL (2015) Acta Crystallographica C, 71,
504 3-8.

505 Shimazu, M., Mizota, T. (1972) Levyne and erionite from Chojabaru, Iki island, Nagasaki Pref.,
506 Japan. The Journal of Japanese Association of Mineralogists, Petrologists and Economic
507 Geologists, 67, 418-424.

508 VandeVondele, J., Hutter, J. (2007) Gaussian basis sets for accurate calculations on molecular
509 systems in gas and condensed phases. Journal of Chemical Physics, 127, 114105.

510 VandeVondele, J., Krack, M., Mohamed, F., Parrinello, M., Chassaing, T., Hutter, J. (2005)a
511 Quickstep: Fast and accurate density functional calculations using a mixed Gaussian and
512 plane waves approach. Computer Physics Communications, 167, 103-128.

513 VandeVondele, J., Mohamed, F., Krack, M., Hutter, J., Sprik, M., Parrinello, M. (2005)b. The
514 influence of temperature and density functional models in ab initio molecular dynamics
515 simulation of liquid water. Journal of Chemical Physics 122: 014515.

516 Velazquez-Peña, G. C., Solache-Ríos, M., Olguin, M. T., Fall, C. (2019) As(V) sorption by different
517 natural zeolite frameworks modified with Fe, Zr and FeZr. Microporous and Mesoporous
518 Materials, 273, 133-141

519 Wang, S., Peng, Y. (2010) Natural zeolites as effective adsorbents in water and wastewater
520 treatment. Chemical Engineering Journal, 156, 11-24.

521 Wise, S. W., Tschernich, R., W. (1976) The chemical composition and origin of the zeolites
522 offretite, erionite and levyne. American Mineralogist, 61, 853-863.

Yamamoto, K., Ikeda, T., Onodera, M., Muramatsu, A., Mizukami, F., Wang, Y., Gies, H. (2010) Synthesis and structure analysis of RUB-50, an LEV-type aluminosilicate zeolite. Microporous and Mesoporous Materials, 128, 150-157.

Zhu, G. S., Xiao, F. S., Qiu, S. L., Hun, P. C., Xu, R. R., Ma, S. J., Terasaki, O. (1997) Synthesis and characterization of a new microporous aluminophosphate with levyne structure in presence of HF. Microporous and Mesoporous Materials, 11, 269-273.

Zukal, A., Pulido, A., Gil, B., Nacthtigall, P., Bludský, O., Rubeš, M., Čejka, J. (2010) Experimental and theoretical determination of adsorption heats of CO_2 over alkali metal exchanged ferrierites with different Si/Al ratio. Physical Chemistry Chemical Physics 12, 6413-6422.

This is the peer-reviewed, final accepted version for American Mineralogist, published by the Mineralogical Society of America.
The published version is subject to change. Cite as Authors (Year) Title. American Mineralogist, in press.
DOI: https://doi.org/10.2138/am-2020-7500. http://www.minsocam.org/

546

547

548 **Table 1** Relevant bond distances (Å) of Ag-levyne structure at room temperature.

Framework					
T1-O4		1.6431(14)	T2-O5 ×2		1.6391(12)
T1-O1		1.645(3)	T2-O1 ×2		1.647(3)
T1-O3		1.6558(16)	<T2-O>		1.643
T1-O2		1.6800(19)			
<T1-O>		1.656			
Extraframework					
Ag1-W1	×3	2.372(8)	Ag4A-O1	×2	2.684(13)
-O2	×3	2.470(5)	-W3	×2	2.77(3)
			-O5	×2	2.765(11)
Ag2-O5	×6	2.591(5)			
Ag2A- O5	×3	2.682(7)			
Ag2B-W3	×3	2.60(3)			
Ag3-W1	×3	2.33(2)			
-W3	×3	2.34(3)			

549

550 **Table 2** Unit-cell parameters of Ag-levyne obtained from MD trajectories and SC-XRD data
551 collected at RT. The deviation (in percentage) of MD unit-cell parameters from those obtained by
552 SC-XRD is shown.

	MD	**XRD**	**Deviation**
a-axis (Å)	13.47(8)	13.4169(3)	0.43%
b-axis (Å)	13.52(8)	13.4169(3)	0.79%
c-axis (Å)	22.98(14)	22.5926(6)	1.75%

This is the peer-reviewed, final accepted version for American Mineralogist, published by the Mineralogical Society of America.
The published version is subject to change. Cite as Authors (Year) Title. American Mineralogist, in press.
DOI: https://doi.org/10.2138/am-2020-7500. http://www.minsocam.org/

α (°)	90.16	90	0.17%
β (°)	89.90	90	0.11%
γ (°)	119.99	120	0.009%
Cell volume (Å^3)	3621(13)	3522.09(18)	2%

Table 3 Relevant bond distances (Å) of Ag-erionite structure at room temperature.

Framework				
T1-O1		1.651(2)	T2-O3	1.6231(18)
T1-O2		1.634(2)	T2-O4 ×2	1.649(4)
T1-O4		1.649(4)	T2-O5	1.646(3)
T1-O6		1.650(2)	<T2-O>	1.642
<T1-O>		1.646		
Extraframework				
K1-O1	×6	2.941(6)	C3-W4A ×2	2.63(2)
K1A –O1	×3	2.51(11)		
K1A –O6	×3	3.09(17)		
C1-O6	×2	2.500(6)		
-O4	×2	2.986(5)		
C2-O5	×3	2.487(11)		
C2A-O5	×3	2.410(10)		
C2B-O5	×3	2.640(14)		
-W5		2.29(6)		

573

574

575

576

577

578 **Figure Captions**

579

580 **Figure 1** SEM BSD images of levyne-erionite intergrowths.

581

582 **Figure 2** Crystal structure of Ag-levyne projected along [110]. Blue spheres represent the (Si,Al)
583 tetrahedral sites, silver and oxygen atoms are displayed in grey and red, respectively. Partially
584 colored spheres correspond to partial occupancy of the crystallographic sites. The yellow line
585 indicates the three-fold axis.

586

587 **Figure 3** A snapshot of Ag-levyne structure after 18 ps MD simulation. Color code as in Figure
588 2. Al-occupied tetrahedral sites are shown as dark cyan spheres. Ag-O bonds are shown with
589 grey lines.

590

591 **Figure 4** Radial distribution function (RDF) (continuous line) and coordination number (CN)
592 (dotted lines) of Ag-O and Ag-Ow distances of Ag-levyne calculated from MD trajectories.

593

594 **Figure 5** Silver and water molecules distribution within the *lev* cavity of the (a) calculated
595 (snapshot after 18 ps calculation) and refined (b) Ag-levyne structure.

596

597 **Figure 6** Crystal structure of Ag-erionite refined from XRD. Color code as in Figure 2. Purple
598 spheres represent K atoms. Grey lines indicate Ag-O bonds in the *eri* cavity.

599

600 **Figure 7** Perspective view of the **s**imulated (11 ps) Ag-levyne supercell with 2 H_2O per Ag ions.
601 Color code as in Figure 3. Ag ions are not found in the D6R cages.

Figure 1

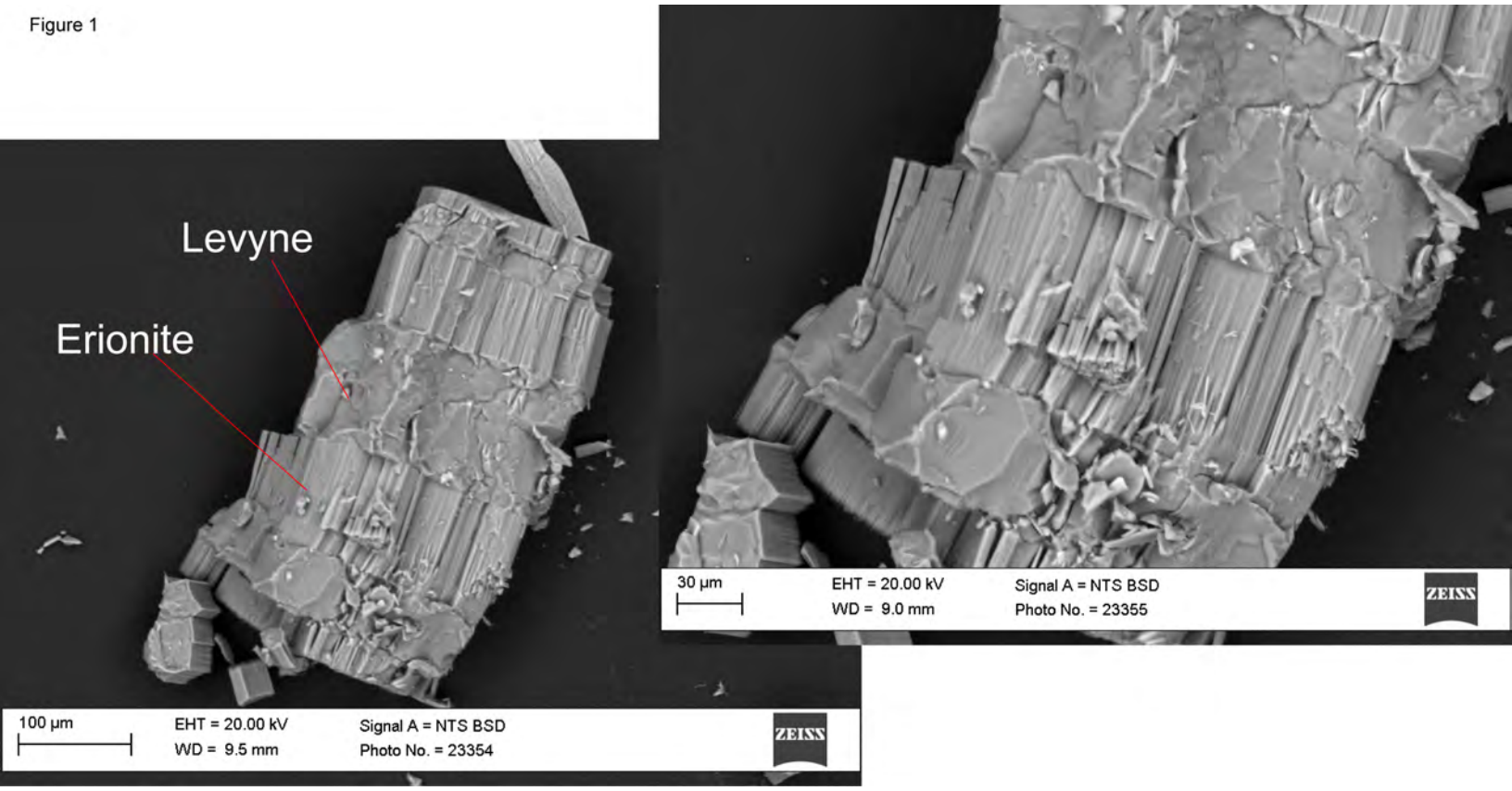

This is the peer-reviewed, final accepted version for American Mineralogist, published by the Mineralogical Society of America.
The published version is subject to change. Cite as Authors (Year) Title. American Mineralogist, in press.
DOI: https://doi.org/10.2138/am-2020-7500. http://www.minsocam.org/

Figure 2

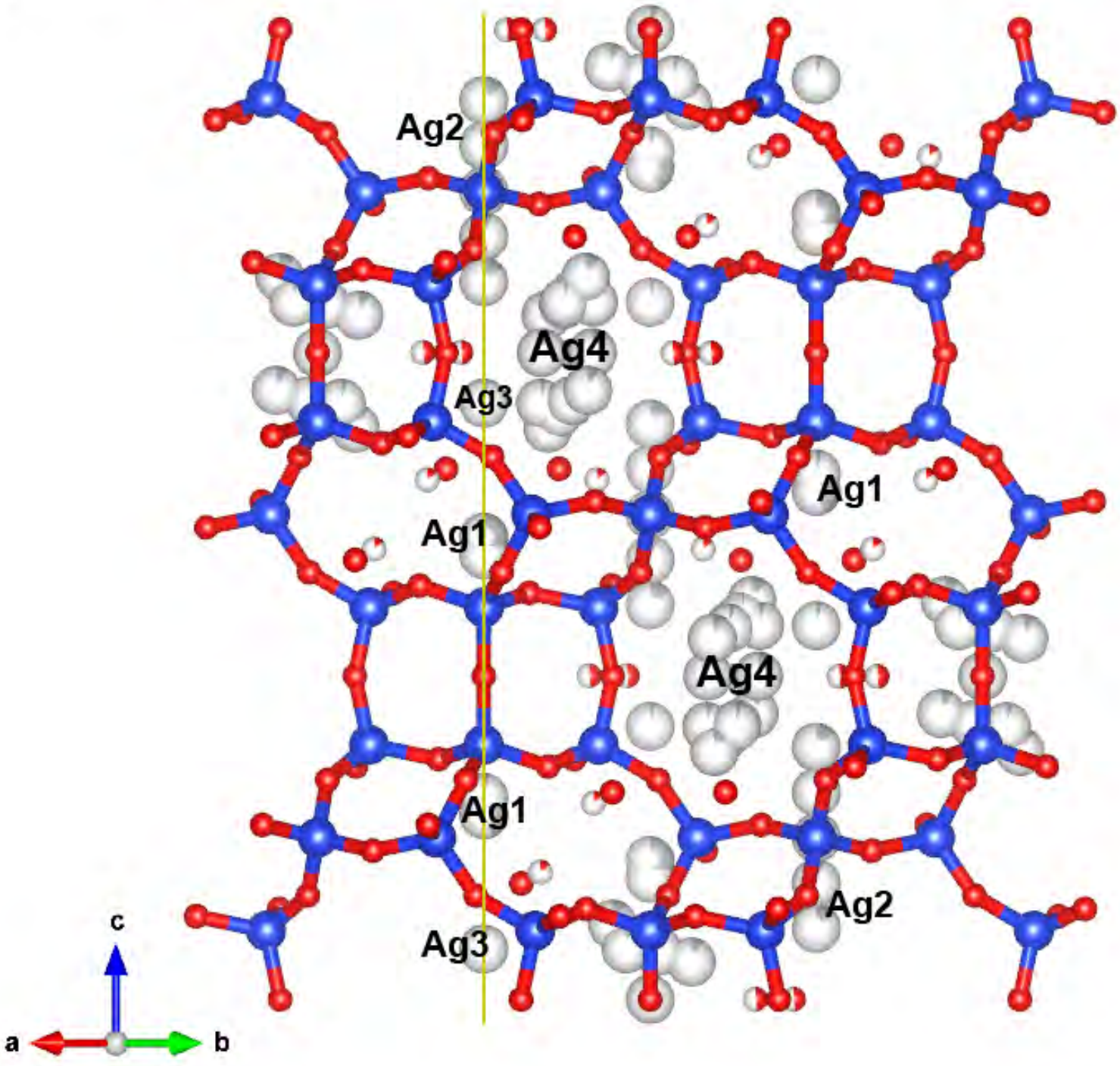

Figure 3

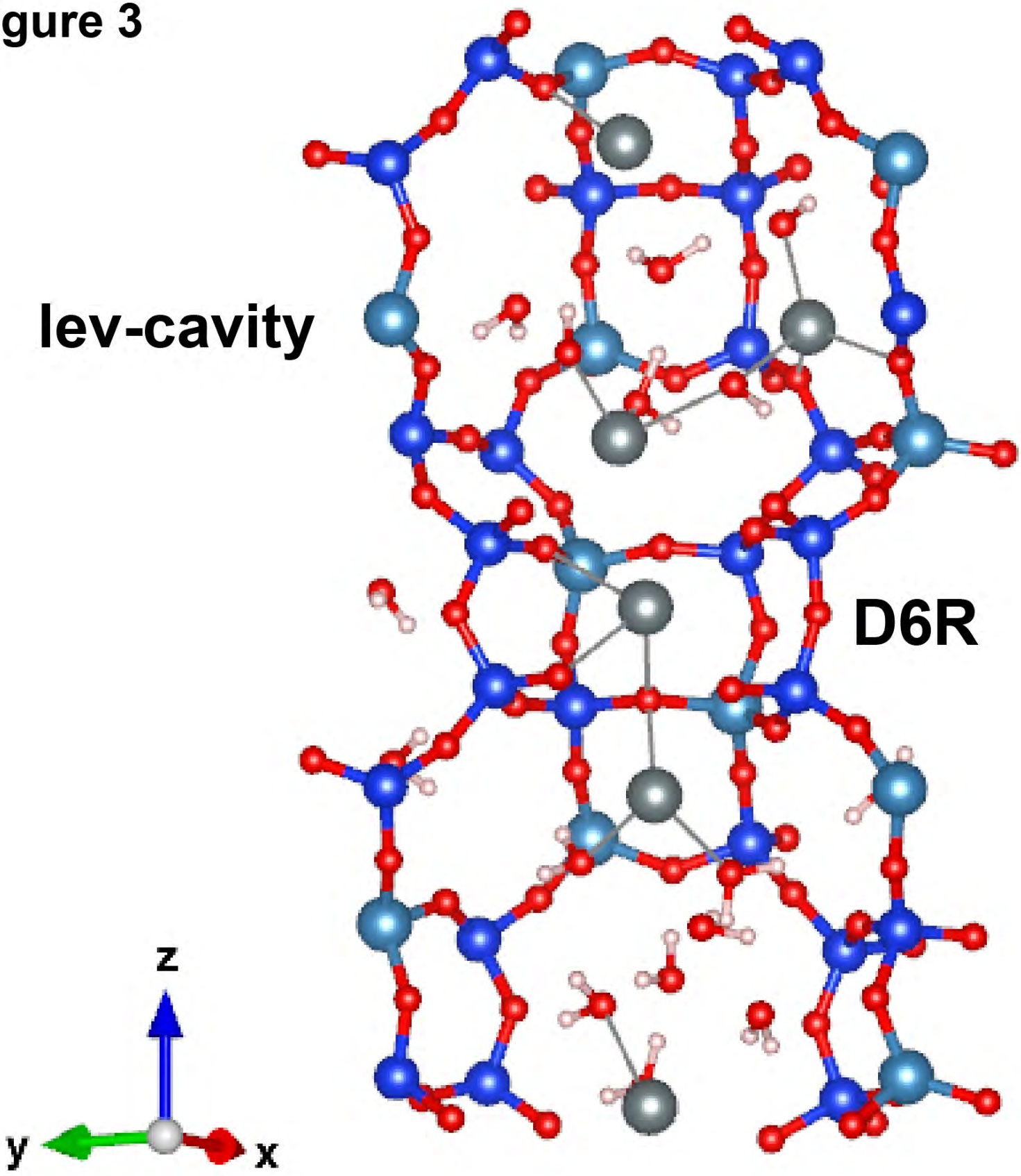

This is the peer-reviewed, final accepted version for American Mineralogist, published by the Mineralogical Society of America.
The published version is subject to change. Cite as Authors (Year) Title. American Mineralogist, in press.
DOI: https://doi.org/10.2138/am-2020-7500. http://www.minsocam.org/

Figure 4

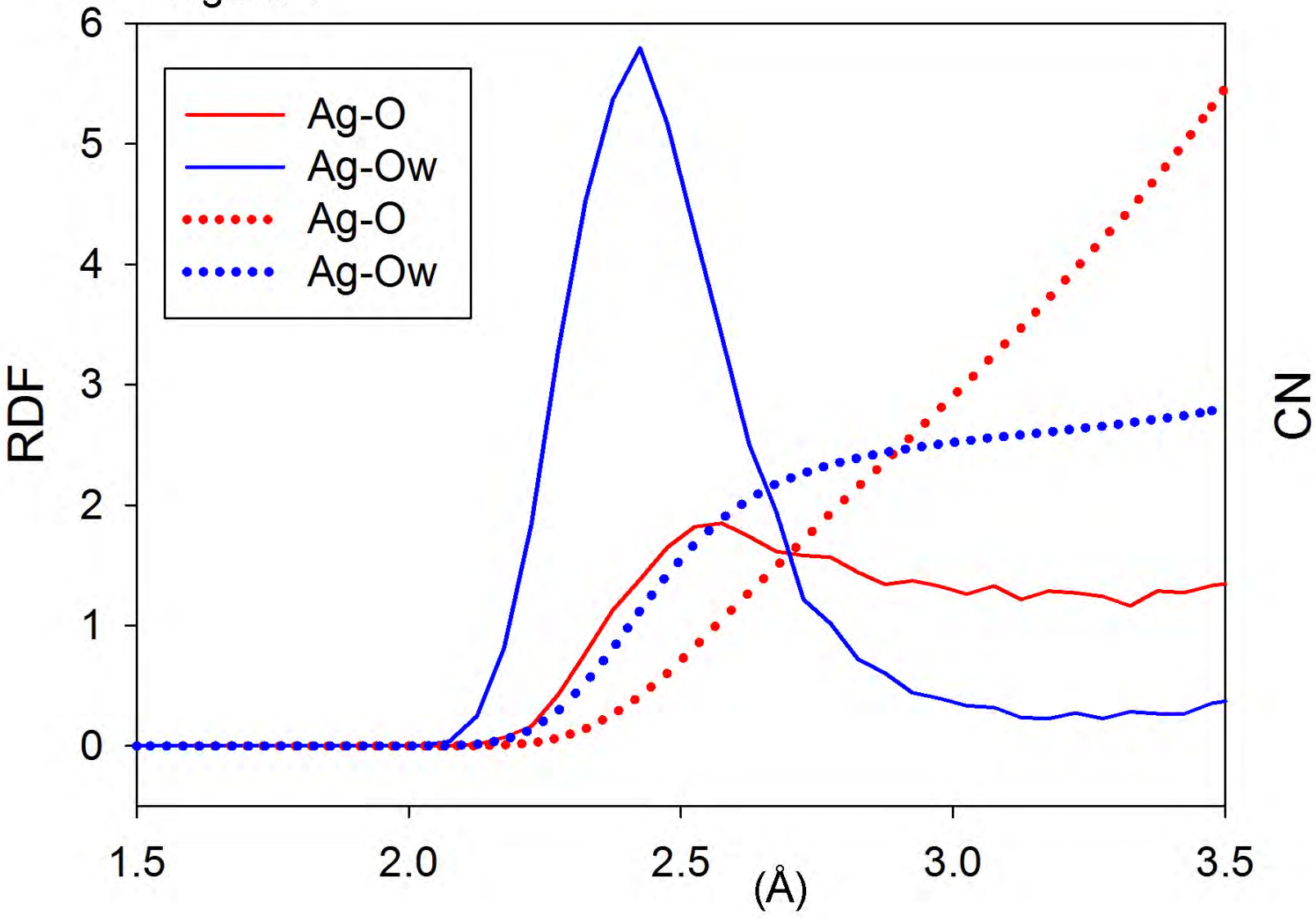

This is the peer-reviewed, final accepted version for American Mineralogist, published by the Mineralogical Society of America.
The published version is subject to change. Cite as Authors (Year) Title. American Mineralogist, in press.
DOI: https://doi.org/10.2138/am-2020-7500. http://www.minsocam.org/

Figure 5

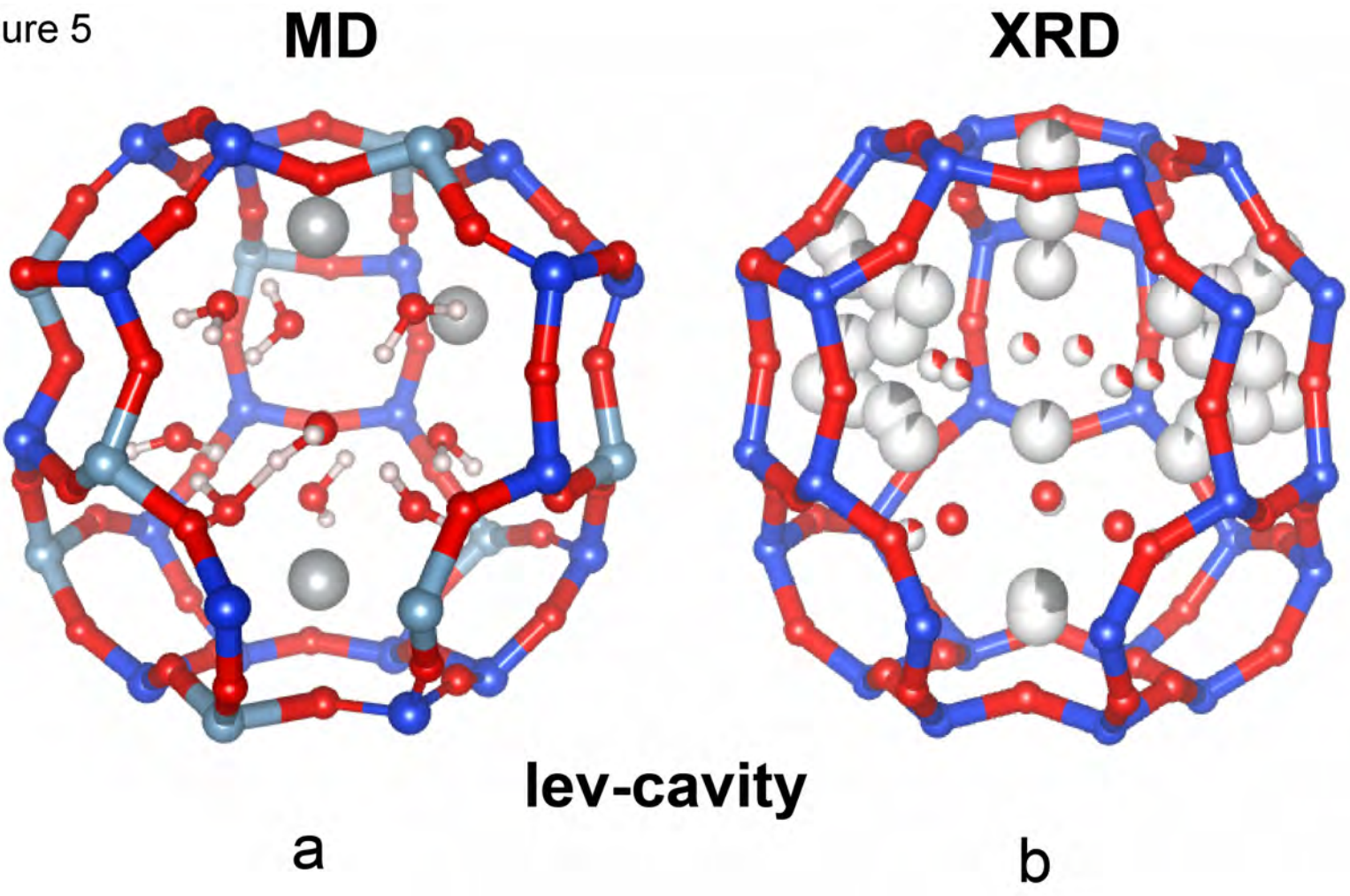

This is the peer-reviewed, final accepted version for American Mineralogist, published by the Mineralogical Society of America.
The published version is subject to change. Cite as Authors (Year) Title. American Mineralogist, in press.
DOI: https://doi.org/10.2138/am-2020-7500. http://www.minsocam.org/

Figure 6

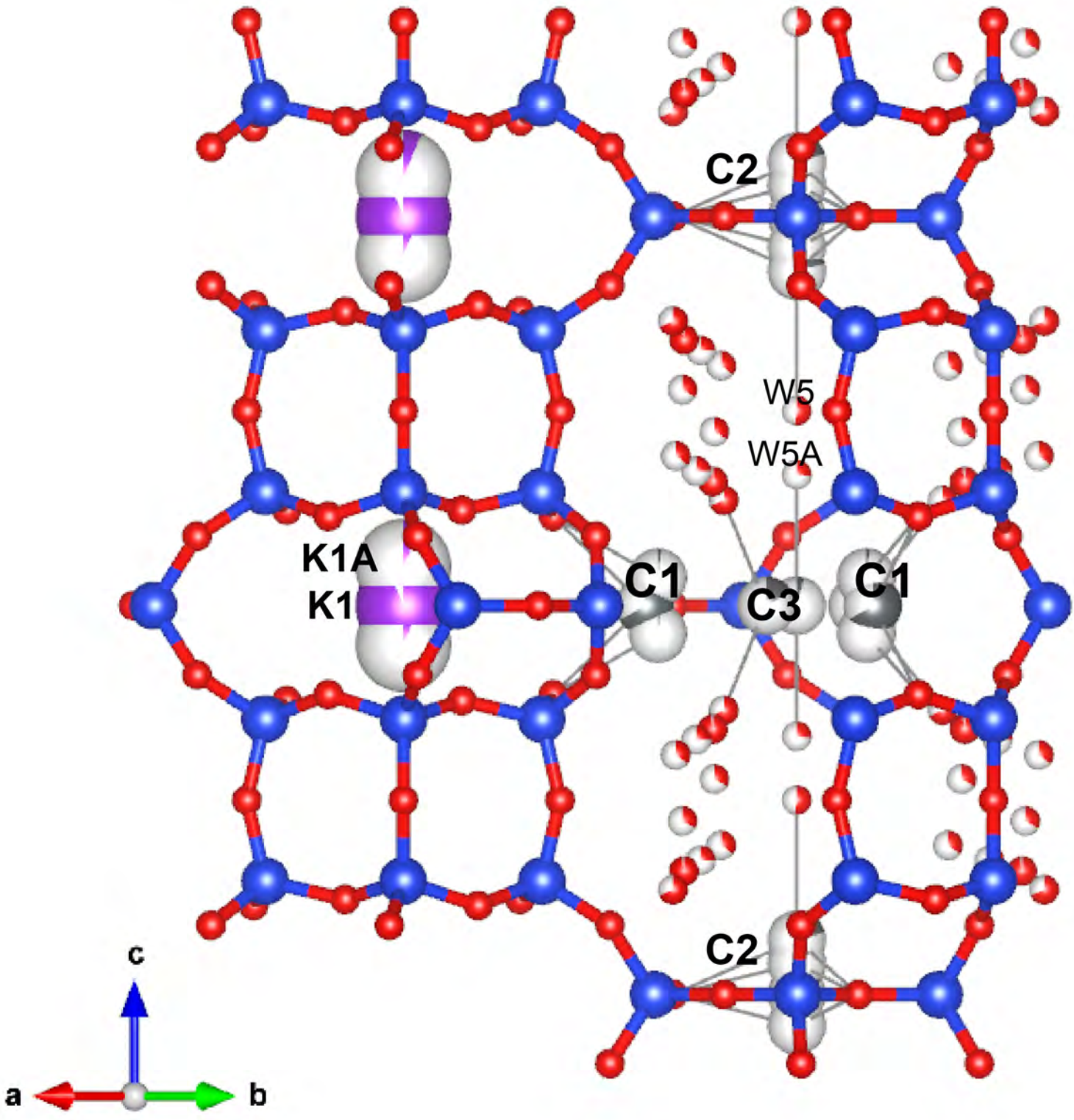

This is the peer-reviewed, final accepted version for American Mineralogist, published by the Mineralogical Society of America.
The published version is subject to change. Cite as Authors (Year) Title. American Mineralogist, in press.
DOI: https://doi.org/10.2138/am-2020-7500. http://www.minsocam.org/

Figure 7